



Matching geometry and stimulation parameters of electrodes for deep brain stimulation experiments—Numerical considerations

Ulrike Gimsa^a, Ute Schreiber^c, Beate Habel^b, Jürgen Flehr^c,
Ursula van Rienen^c, Jan Gimsa^{b,*}

^a University of Rostock, Medical Faculty, Department of Neurology, Gehlsheimer Str. 20, D-18055 Rostock, Germany

^b University of Rostock, Institute of Biosciences, Department of Biology, Gertrudenstr. 11A, D-18051 Rostock, Germany

^c University of Rostock, Faculty of Computer Science and Electric Engineering, Albert-Einstein-Str. 2, D-18051 Rostock, Germany

Received 16 March 2005; received in revised form 17 June 2005; accepted 20 June 2005

Abstract

Deep brain stimulation, the electric stimulation of basal ganglia nuclei, is a treatment for movement disorders such as Parkinson's disease. The underlying mechanisms are studied in animals, e.g. rodents. Designs and materials of commercially available microelectrodes, as well as experimentally applied driving signals vary tremendously. We used finite integration modeling to compare the electric field and current density distributions induced by various electrodes. Current density or field strength "hot spots", which are located particularly at sites of high curvature and material interfaces coincided with corrosion and erosion at poles and insulation, respectively, as shown by scanning electron microscopy of stainless steel electrodes. Cell constants, i.e. geometry factors relating the electrode impedance to the specific medium conductivity, were calculated to determine the electrode voltage for a given stimulation current. Nevertheless, for electrodes of the same cell constant but of different geometry, current and field distributions may be very dissimilar. We found geometry-dependent limiting values of the stimulation current, above which electric tissue damage may occur. These values limit the reach of the stimulation signal for a given electrode geometry. Also, electrode geometries determine the shape of the stimulated tissue volume. This study provides tools for choosing the most appropriate geometry for targeting different-sized brain areas.

© 2005 Elsevier B.V. All rights reserved.

Keywords: Microelectrodes; High-frequency stimulation; Neuromodulation; Rat; Finite integration technique; Field distribution; Electrode impedance

1. Introduction

Before deep brain stimulation (DBS) became a therapy in itself, electric stimulation of basal ganglia had been used to guide neurosurgeons to the precise position for a surgical lesion, the ultimate therapy of late-stage Parkinson's disease (PD). Nowadays, DBS is well established as a symptomatic treatment for PD and other movement disorders. The main advantage of DBS over surgical lesions are its ability to modulate stimulation parameters and its reversibility (Benabid et al., 1987).

Different hypotheses exist to explain the mechanism of DBS. Both neuronal excitation and inhibition are being dis-

cussed (Vitek, 2002; McIntyre et al., 2004). It is still unclear which parameter determines whether neurons are artificially stimulated; the induced transmembrane potential, which is proportional to the tissue field strength, or the activating function (Rattay et al., 2003). Roughly speaking, the activating function considers sites in the vicinity of neurons or axons to be especially vulnerable to artificial stimulation when they are sources or sinks of field, i.e. the sites of charge induction. In a homogeneous external field, such sites will be represented by axon endings or bends. In an inhomogeneous field it will be, e.g. the axonal spots exposed to the strongest field inhomogeneity (Rattay et al., 2003). Considering only the field inhomogeneity but not the tissue and cell structures for the activating function both dependencies will result in certain spatial distributions of the efficiency of neural excitation. For a review of the current knowledge on medical

* Corresponding author. Tel.: +49 381 494 2037; fax: +49 381 494 2039.
E-mail address: jan.gimsa@uni-rostock.de (J. Gimsa).

DBS, please see [Horch and Dhillon \(2002\)](#), [Kuncel and Grill \(2004\)](#).

Unlike other therapies, DBS was not preceded by extensive work in animal models. This might be a reason for a lack of standardization in stimulation protocols and equipment in animal models such as rodents. In addition, no data has so far been published that describes the commercially available electrodes for rodent models, their properties and the field they induce in the target tissue—the central nervous system (CNS). As electrodes of different geometries are available, it is difficult for researchers to choose an appropriate electrode without having detailed information, e.g. on the size of the maximal applicable current, the stimulated tissue region, etc.

While DBS has been continuously applied in patients without signs of tissue damage for years ([Haberler et al., 2000](#); [Henderson et al., 2002](#); [Moss et al., 2004](#)), tissue damage has been observed following long-term stimulation in animals ([Darbaky et al., 2003](#)). This might be the reason why physiological data based on animal models are usually restricted to short-term stimulation. However, a recent study showed that tissue damage is also relevant in short-term stimulation ([Harnack et al., 2004](#)). These findings in animals may have a number of reasons, such as the use of less inert electrode materials, e.g. non-noble metals, the smaller electrode size and blunt edges (higher curvatures) resulting in higher local current densities leading to more intense local electrode reactions. Electrode reactions produce potentially toxic products like denatured proteins, gas, dissolved metal ions and erosion-products of the insulating materials, etc. These reactions are accompanied by so-called “overpotentials” corresponding to the energy that is dissipated in the electrode reactions and thus lost for the electric stimulation of the tissue. We have discussed the consequences elsewhere ([Gimsa et al., 2005](#)). Moreover, tissue damage may also be directly induced by electric cell membrane poration at sites of high electric field strength over a very short time ([Suzuki et al., 1998](#)). Potential sites are field hot spots near the electrode surface. The field strength at these hot spots thus imposes a criterion for the maximum current or voltage that can be applied to an electrode of given geometry.

The classical way of describing the field distribution induced by electrodes of complex geometries is to directly measure potentials on enlarged electrode models suspended in a water-filled trough; see [Gimsa et al. \(1988\)](#) for example. Today, numerical techniques are state-of-the-art. They allow for a fast and very accurate solution of Maxwell’s equations even for very complex geometries. Maxwell’s equations describe the properties of electromagnetic fields by a system of coupled partial differential equations for the electric and magnetic field quantities. There are different approaches for the numerical solution of electromagnetic field problems, e.g. Boundary Element Methods, Finite Elements Methods (FEM) or Finite Difference Methods. Each of these methods has its pros and cons. The Finite Integration Technique (FIT) ([Weiland, 1977](#); [Schuhmann et al., 1996](#)) is used throughout

this manuscript. Like FEM, FIT is a volume-oriented method, i.e. the whole space considered in the computation is filled by small finite volumes of tetrahedrons or cuboids. A special feature of FIT is that it consistently transfers Maxwell’s equations into linear operator equations on the grid. Here, consistency means that all vector-analytical and physical properties of the fields still hold on the grid (see [Appendix A](#)). Thus, energy conservation and most of the other properties are correctly reflected by the discrete solution. For details, see [Appendix A](#).

For fully three-dimensional electrode models, FIT allows for describing the spatial potential, current density, field distributions, etc. Our calculations have been aimed at describing commercially available concentric microelectrodes of different geometries which are or can be used in animal DBS experiments, especially the stimulation in rats. Our intentions were:

1. to describe the inhomogeneous current density distributions at the electrode surfaces causing a variation in the intensity of the electrode reactions and to localize probable hot spots of metal corrosion and erosion of the insulating parts;
2. to calculate field hot spots as the potential sites of electrically induced tissue damage by membrane poration;
3. to calculate the maximally applicable current (or voltage) still avoiding membrane poration in dependence on the medium conductivity;
4. to calculate cell constants which are the geometry factors relating the impedance of the electrodes to the specific conductivity of the surrounding medium;
5. to describe the spatial distribution of the efficiency of neural excitation by the spatial distributions of the electric field strength and the activating function around the various electrodes.

This manuscript is a continuation of our study on microelectrodes for animal DBS experiments, demonstrating their electrochemical particularities ([Gimsa et al., 2005](#)). Our current analysis provides information beyond that disclosed by the electrode manufacturers. This information is indispensable for researchers who want to choose the optimal electrode geometry for specific CNS targets.

2. Materials and methods

2.1. Electrode properties

In the following, we consider concentric bipolar microelectrodes of different geometries as summarized in [Table 1](#).

An ideal electrode behavior (no potential drop at the metal/medium interface by electrochemical electrode processes) and a constant potential at each site of a metallic surface were assumed for calculations.

Table 1
Electrode characteristics

Electrode type	Abbreviation	Geometry of the two poles ^a	Company	Diameter (μm)	
				Outer pole	Inner pole
SNEX-100, bipolar	Sx(b)	Stacked	RMI	250	100
SNEX-100, unipolar	Sx(u)	–	RMI	250	100
CB CSG 75	S75	Stacked	FHC	250	75
CB CEG	E	Elongated	FHC	250	75
CB CFG	F	Flat	FHC	250	75
CB ASC 25	S25	Stacked	FHC	125	25
CB CPG	P	Pencil-shaped	FHC	125	25
CB CRG	R	Round	FHC	125	25

RMI: Rhodes Medical Instruments Inc., Tujunga, CA, USA. FHC: FHC Inc., Bowdoinham, ME, USA.

^a Electrode geometries are depicted in Fig. 2.

2.2. Numerical modeling and image processing

Calculations were performed on three-dimensional electrode-medium models using the FIT discretization method. The electrodes were described by three-dimensional bodies which are surrounded by a homogenous volume conductor representing the tissue. Three different materials were introduced, metallic surfaces described by the applied potential, and the insulating epoxy of the electrodes and the aqueous electrolyte solution described by their conductivities (10^{-12} and 1.5 S/m , respectively) and relative permittivities (4, 80). The number of grid nodes equaling the number of equations was varied from 600,000 to 1,000,000. The surrounding medium was assumed to be homogeneous and isotropic and to possess aqueous properties. Nevertheless, an assumption of modified properties could only introduce minor changes in the obtained distributions. The reason is that the other two materials in the system (metal and insulating plastics) possess contrasting properties which both strongly differ from those of the brain tissue.

FIT was originally developed for the numeric solution of the complete system of Maxwell's equations in full generality (Weiland, 1977). It provides a consistent scheme for transferring Maxwell's equations in integral form onto a pair of grids, e.g. Cartesian grids. The potential, field strength and flux are assigned to the grid nodes, edges and facets, respectively. The primary and dual grids are coupled via the material parameters of conductivity, permittivity and permeability. Maxwell's equations lead to systems of linear equations for each single grid cell, the so-called Maxwell's grid equations (Schuhmann et al., 1996). One of the advantages of FIT is in keeping the inherent properties of Maxwell's equations for Maxwell's grid equations, leading to a benign behavior with respect to stability and convergence. For the electrode problems studied here, the complexity of the problem can be reduced applying the electro-quasistatic (EQS) approximation for time harmonic fields. Please refer to the Appendix A for a short introduction, for further details, see Haus and Melcher (1989), van Rienen (2001).

In practice, the discretization of the models and the calculations of electric field and current density distribution have been performed with the MAFIATM computer aided engineering (CAE-) tool (Version 4.106, CST GmbH, Darmstadt, Germany) which is based on FIT. MAFIATM was used on a SUN Enterprise 450 with four 300 MHz processors and 4 Gbyte RAM. The solution domain was $1 \text{ mm} \times 1 \text{ mm} \times 1.3 \text{ mm}$, which gives a boundary-electrode-distance of at least three times the outer electrode radius. The step size in and near the electrodes was adjusted until it was smaller than $2 \mu\text{m}$, since the approximation error grows with the square of the step size while the rounding error and the influence of the boundaries are negligible. The mesh size has been optimized by starting with a coarser mesh and refining it until the result converged. For 800,000 grid points the CPU time was about 2 h. Post-processing was performed using MATLABTM V6.5. This included computation of all problem-specific constants such as the maximum transmembrane potentials, the volumes of stimulated tissue, the cell constants as well as the preparation of figures.

2.3. Calculation of field distribution in the tissue

To consider the affected tissue volume and the homogeneity of the field distribution, we calculated the distributions of potential, electric field, current density and activating function at the electrode's metallic and insulating surfaces and in the surrounding medium, i.e. the brain tissue. In an initial calculation, potentials of 1 and 0 V, respectively, have been assumed at the inner and outer poles of the electrode for each electrode geometry. Calculations have been conducted for a harmonic field of 130 Hz—the repetition rate of a standard DBS pulse and the basic frequency of the Fourier series (for details, see Gimsa et al., 2005).

The electric potential, the electric field strength and the current density distributions as well as the overall tissue current were calculated. Assuming the system to be linear and homogeneous, the obtained current was then rescaled to $500 \mu\text{A}$. The scaling factor, i.e. the potential difference for a current of $500 \mu\text{A}$ for each of the investigated electrode geometries is presented in Table 3.

3. Results

3.1. Spatial field distribution in the tissue

The spatial distribution of the electric field in brain tissue is most important for DBS effects. The coaxial electrodes used in animal experiments exhibit inhomogeneous distributions of the fields, the potentials and the current densities (Fig. 1A–C, respectively). In homogeneous media of linear properties, the field strength (V/m) is proportional to the current density (A/m^2) and the specific resistance, i.e. the inverse of the specific conductivity, σ (S/m). The field inside the insulation region is much higher than in the aqueous solution. In solution, the local field maxima were found at sites of

strongest metal curvature. High fields can also be observed at the so-called (material) triple-points, i.e. sites where the three interfaces of metal, insulation and solution join. In comparison to the aqueous medium, the insulation material does not weaken the field generated by the electrode. The aqueous medium has a high permittivity and conductivity compared to the insulating material and can, therefore, act as a virtual electrode protruding towards the insulation (see arrows in Fig. 1A). This effect leads to additional field maxima near the solution–insulation interfaces. Because the current density at the electrode surface is directly related to the rate of electrochemical reactions, it is also related to increased corrosion or erosion at sites of high current density (compare to Figs. 7 and 8) (Gimsa et al., 2005).

3.2. Electrode geometry factor (cell constant)

The current induced by a certain (dc-) electrode voltage is proportional to the electrode conductance G (S). G or electrode resistance R (Ω) = $1/G$ (S) determine the relation of electrode voltage and current according to Ohm's law. Please note, that in practice the electrode impedance Z (Ω), i.e. the frequency-dependent resistance has to be taken into account.

As an example, Z of a chamber made of two coplanar electrodes of the same area, A , positioned at distance, d , should be considered. According to Ohm's law, Z is determined by the voltage, U , over the electrodes and the current, I , through the medium in between the electrodes (Eq. (1)):

$$Z = \frac{U}{I} = \frac{d}{\sigma A} = \frac{1}{\sigma \gamma} \quad (1)$$

The ratio A/d can be summarized by the cell constant, γ (m), that can also be derived for chambers of complex geometries. For electrodes of given arbitrary shape γ linearly increases with a characteristic dimension. For a given current, the electrode voltage will depend on γ and the medium of conductivity σ (S/m).

Obviously, γ is an important parameter for adjusting the stimulation current in DBS. For complex electrode geometries, γ can be determined numerically. Mathematically, γ has been calculated from the overall current emanating from the inner and flowing to the outer electrode at a given potential difference. The overall current has been obtained by integration over a closed surface around the inner electrode. In the geometric FIT model the metallic surface of the center electrode was encapsulated by a box-sized closed surface that had roughly the dimension of the electrode tip. We found that a positioning of the borders of the surface a short distance away from the center electrode prevented numerical problems and led to more reproducible numerical results. The current was then determined by the surface integral of the current density. Since electrode potential difference and medium conductivity were assumed, γ could immediately be derived from the current. The factor γ of each microelectrode relates electrode voltage and current for any medium conductivity. Results are given in Eq. (1) and Table 2.

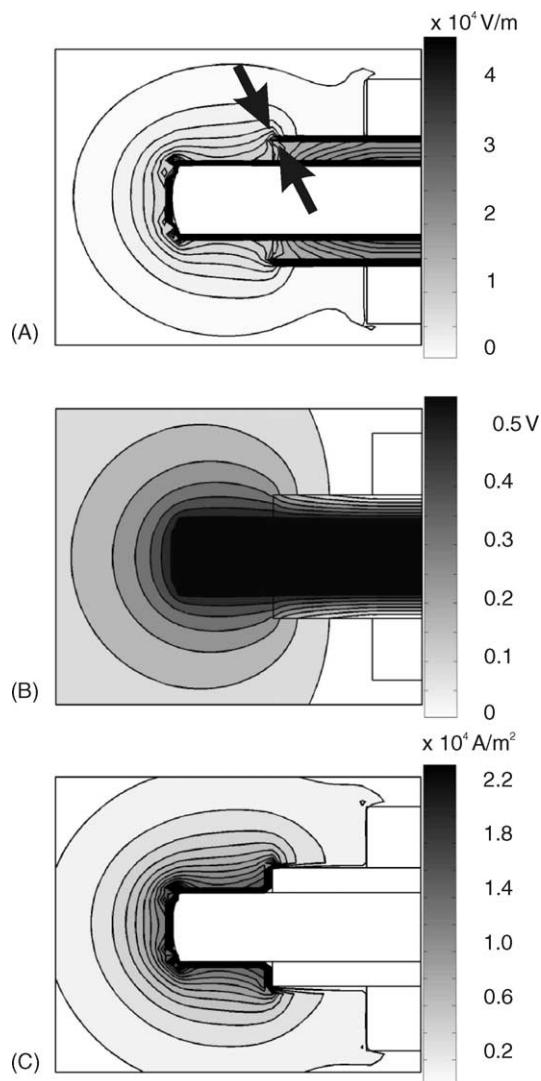


Fig. 1. Magnitudes of electric field strength (A), potential (B) and current density (C) for an S75 electrode shown in gray scales. The inner and outer poles of the electrode were set to 1 and 0 V, respectively, for calculations. The field inside the insulation region is orders of magnitude higher than in the aqueous solution. Arrows depict additional field maxima near the solution–insulation interfaces.

Table 2

Numerically calculated impedances and cell constants of different electrode geometries assuming a medium conductivity of 1.5 S/m

Electrode type	Diameter of inner pole (μm)	Impedance Z (k Ω)	Cell constant γ (mm)
Sx(u)	100	0.686	0.97
Sx(b)	100	0.700	0.95
S75	75	1.181	0.56
E	75	2.210	0.30
F	75	2.304	0.29
S25	25	2.463	0.27
P	25	5.844	0.11
R	25	10.310	0.065

3.3. How much tissue is reached by stimulation?

The induced transmembrane potential and the activating function are commonly discussed as criteria for neuronal activation (Kuncel and Grill, 2004). The transmembrane potential is proportional to the field strength induced in the tissue. According to Rattay et al. (2003), the activating function is the second derivative of the electric potential along a straightened axon. In the following, both criteria will be considered.

The field strength distributions, i.e. the ranges and focuses of the electric field, have been found to be strongly influenced by the shape of the electrode tip (see Fig. 1A). For a comparison of the various electrode designs, the current relation (Eq. (1)) and cell constants (Fig. 2) were used to rescale the electrode voltages after a first calculation. The rescaling criterion was an electrode current of 500 μA , the stimulation current mostly applied in animal models of DBS. Finally, the field distributions around all the electrode geometries were recalculated. Fig. 3 illustrates these current-normalized field distributions by representative field strength isolines.

Analysis of local values clearly shows big differences in the maximum field strength, the field gradient and the distance over which the tissue will be affected.

To determine the tissue volume affected by a 500 μA stimulation pulse, we assumed the neuronal bodies to be spherical with a radius of 5 μm and immersed in an electrically homogeneous medium. The maximum transmembrane potential $\Delta\Psi$ induced in a cell with negligible membrane conductivity can be estimated by:

$$\Delta\Psi = 1.5 E_{\text{ext}} r \quad (2)$$

with E_{ext} and r being the absolute value of the extracellular field strength and the radius, respectively. $\Delta\Psi$ is the absolute value induced at the cell poles oriented in field direction. Clearly, Eq. (2) may provide only a crude estimate for tissue cells. Nevertheless, a correct description will mainly alter the factor of 1.5 and lead to a correction in the scaling but not in the qualitative result. Fig. 4 shows a calculation of the induced transmembrane potential of neurons in the vicinity of electrodes of different geometries at a stimulation pulse of 500 μA . The isolines represent the spatial limits for an induced transmembrane potential of 10 and 1 mV, corresponding to field strengths of 1.33 kV/m and 133 V/m, respectively.

Please note the additional line close to the electrode surface of the electrodes P and R indicated by arrows. This line represents a field strength of 133 kV/m, inducing a $\Delta\Psi$ of 1 V, a potential generally seen as “critical” for inducing membrane poration and possible irreversible cell damage. In order not to exceed 133 kV/m, stimulation currents have to be limited in dependence on the electrode geometry. Results applying this criterion are given in Table 3. It shows maximum currents that can be applied while still avoiding tissue damage by membrane poration. In essence, different electrode geometries require and allow for different stimulation parameters.

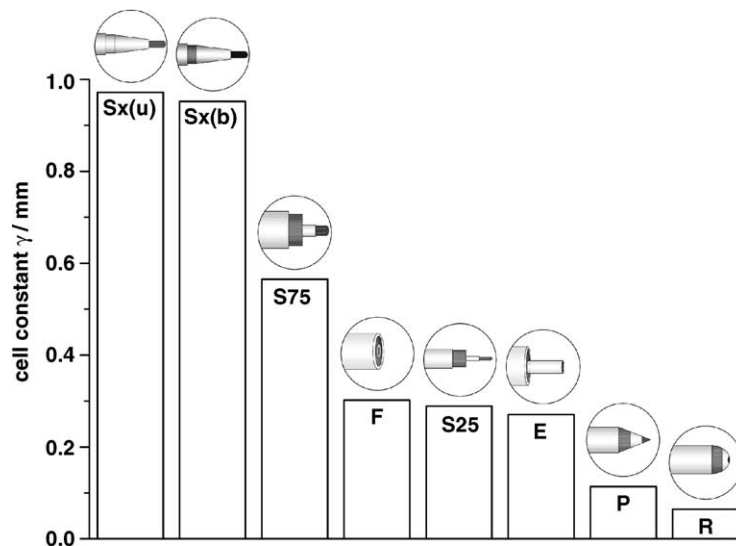


Fig. 2. Cell constants linking electrode voltage and current calculated for different electrode designs (see inserts above columns).

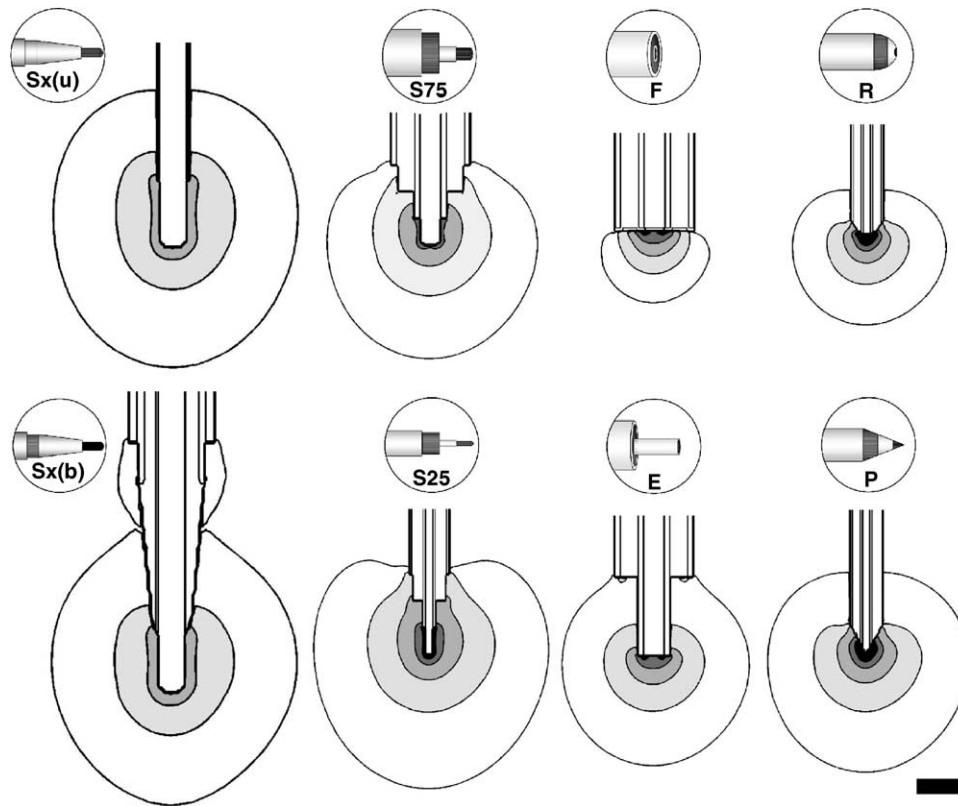


Fig. 3. Spatial field distribution and reach for different electrode geometries (see inserts) in aqueous solution (1.5 S/m). Cell constants have been taken into account to normalize the stimulation current to 500 μA . Isolines in figures delimit field strengths of 0.125, 0.5, 2, 8 and 32 kV/m towards the electrode surface. Please note that field strengths of 8 and 32 kV/m do not occur in the graphs of Sx(u) and Sx(b). Scale bar: 200 μm .

Fig. 5 demonstrates the extent of the stimulation in the tissue under this limiting condition for the different electrode geometries. The actual volumes of stimulated tissue are listed in Table 4.

The activating function was originally defined along straightened axons (Rattay et al., 2003). Since the orientation of the nerve fibers (axons) is not known, a random orientation

was assumed for simplicity (compare to: Kuncel and Grill, 2004). The absolute value of the second spatial derivative of the potential was calculated assuming a stimulating current of 500 μA (Fig. 6). This means that the stimulation of axons with a “correct” orientation is described according to the model of Rattay et al. (2003).

3.4. Current density distribution at the electrode surface

Membrane poration is, however, not the only hazard that must be considered. Fig. 7 illustrates the local distribution of the current density at the electrode surface. Sites of high values must be expected to undergo increased metallic corrosion or plastic erosion (Gimsa et al., 2005). Fig. 7 demonstrates that the electrode tip and both electrode–insulation interfaces are especially exposed (see below).

3.5. Metal corrosion and plastics erosion

Different electrode processes may occur when applying electric fields via metal electrodes to electrolyte solutions such as interstitial fluid: gas evolution, redox-reactions of the organic solution compounds and dissolution of the electrode metal (Agnew and McCreery, 1990; Anderson and Weiland, 2002; Gimsa et al., 2005). We used scanning elec-

Table 3
Stimulation parameters for different electrode types

Electrode type	Electrode voltage (V) to obtain constant current of 500 μA	Maximum $\Delta\psi$ (V)	Maximum applicable current (μA)
Sx(u)	0.34	0.261	1919
Sx(b)	0.35	0.139	3600
S75	0.59	0.148	3378
E	1.10	0.341	1468
F	1.15	0.386	1296
S25	1.23	0.684	731
P	2.92	(1.998)	250
R	5.16	(2.611)	191

The induced transmembrane potential $\Delta\psi$ was calculated using Eq. (2). The Table shows the maximum $\Delta\psi$ that could be induced by 500 μA constant current stimulation. A $\Delta\psi = 1\text{ V}$ limits the maximum applicable current as membrane poration will be induced above this value. Please note that $\Delta\psi > 1\text{ V}$ cannot be reached in practice, as membrane poration will result in a down-regulation of $\Delta\psi$ by an increase in membrane conductance.

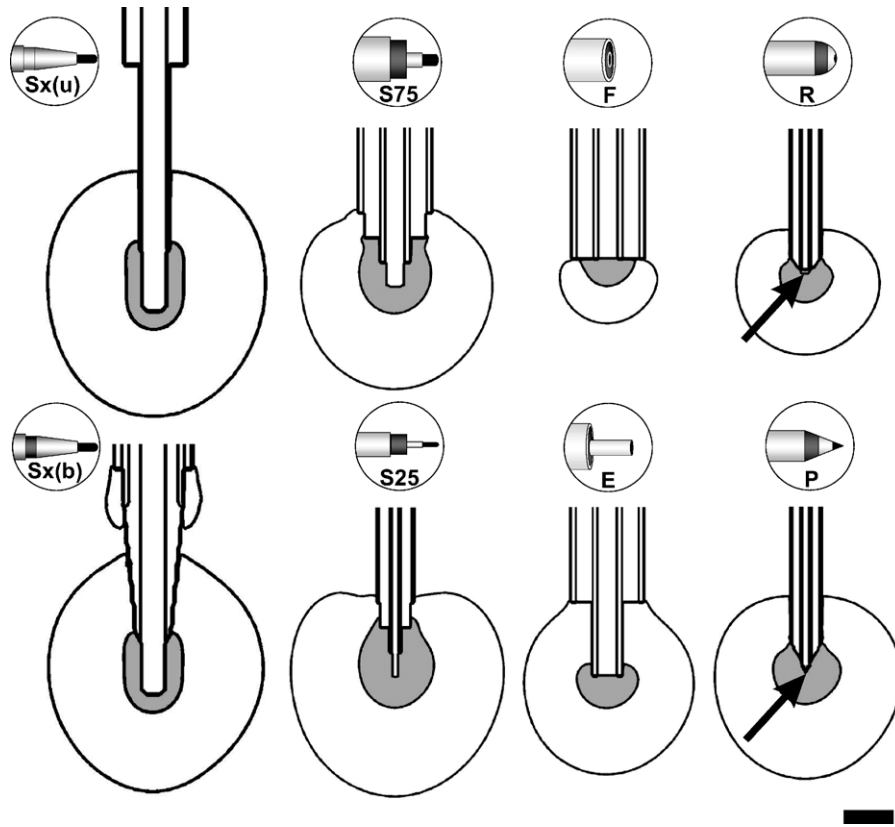


Fig. 4. Different geometries allow for a stimulation of different-sized brain areas. Spatial distribution of induced transmembrane potentials caused by a 500 μ A stimulation current applied at different electrode geometries. The solid lines delimiting white and gray filled areas represent the 10 and 1 mV limits for the induced transmembrane potential, respectively. Please note that at the R and P electrodes, an additional line delimits 1 V (arrows). Maximum transmembrane potentials that can be induced by 500 μ A stimulation at the electrode surfaces are shown in Table 3. Scale bar: 200 μ m.

tron microscopy to check corrosion and erosion of SNEX-100 electrodes (Sx(b)) driven in a bipolar mode. Comparing the results of numerical simulation (Fig. 7) with scanning electron micrographs taken from new (Fig. 8, left panels) and electrodes that had been continuously used for about 8 h (Fig. 8, right panels) gave strong evidence for a current density-dependent corrosion. The overview in Fig. 8A shows strong metal corrosion at the inner pole of the electrode, especially at the base of the electrode tip and plas-

tic erosion of the insulation between outer and inner pole which was most severe close to the inner and outer poles. Looking in more detail (Fig. 8B), a considerable amount of metal had been dissolved from the electrode tip especially towards the insulation. Higher resolution revealed that the metal surface of the tip electrode (Fig. 8C) had changed from smooth to corrugated. The most dramatic deterioration of material quality was observed at the epoxy insulation (Fig. 8D).

Table 4
Electrode geometry determines the volume of stimulated tissue

Electrode type	Tissue volume (mm ³) where the induced transmembrane potential is			
	Between 1 V and 10 mV	Between 1 V and 1 mV	>1 V	Between 1 V and 10 mV*
Sx(u)	1.13×10^{-2}	4.11×10^{-1}	0	8.19×10^{-2}
Sx(b)	1.04×10^{-2}	3.98×10^{-1}	0	20.0×10^{-2}
S75	1.36×10^{-2}	2.26×10^{-1}	0	6.51×10^{-2}
E	0.57×10^{-2}	1.74×10^{-1}	0	1.45×10^{-2}
F	0.27×10^{-2}	0.24×10^{-1}	0	0.41×10^{-2}
S25	1.64×10^{-2}	3.35×10^{-1}	0	1.36×10^{-2}
P	0.86×10^{-2}	0.21×10^{-1}	9.82×10^{-6}	0.16×10^{-2}
R	0.38×10^{-2}	0.84×10^{-1}	1.14×10^{-5}	0.05×10^{-2}

Columns 2–4 show the tissue volume where different transmembrane potentials $\Delta\Psi$ are induced by constant current stimulation of 500 μ A. Please note that column 2 also includes areas where $\Delta\Psi$ exceeds 1 V. The last column* gives the tissue volumes that can be stimulated by the maximum current that induces $\Delta\Psi \leq 1$ V at each site of the tissue.

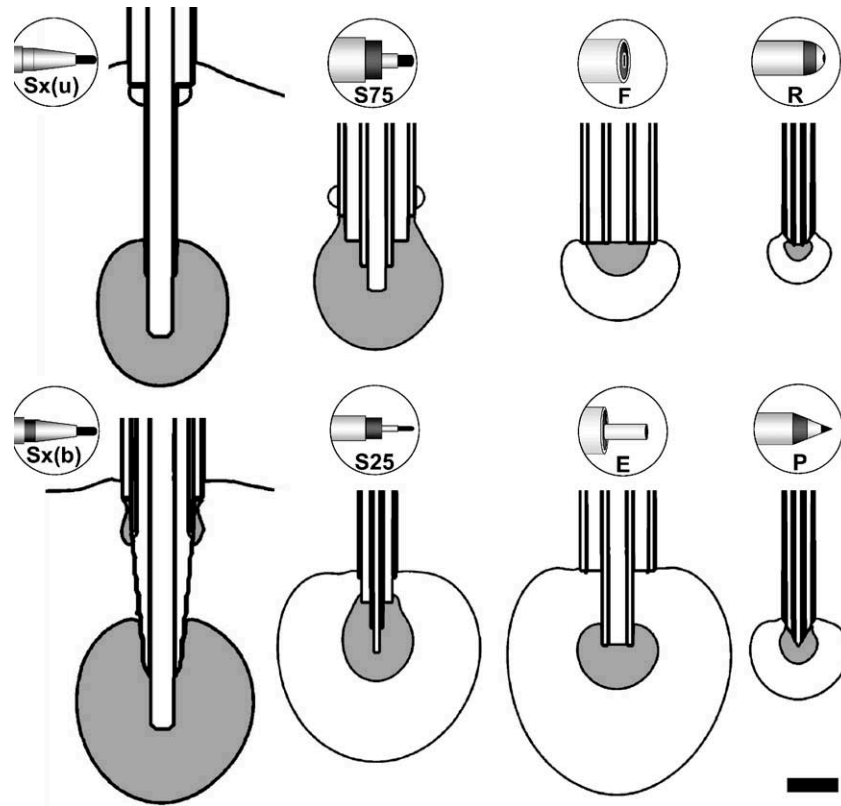


Fig. 5. Different geometries allow for a stimulation of different-sized brain areas. Spatial distribution of induced transmembrane potentials when a maximum of an induced transmembrane potential of 1 V is set as a limit at the electrode surface; maximum stimulation currents for this condition are shown in Table 3. The solid lines delimiting white and gray filled areas represent the 10 and 1 mV limits for the induced transmembrane potential, respectively. Please note that the 1 mV lines around Sx(u) and Sx(b) are not fully depicted. Scale bar: 200 μ m.

4. Discussion

4.1. General remarks

The effects of electric fields on CNS tissue have been modeled extensively (Grill and Mortimer, 1996; Grill, 1999; McIntyre and Grill, 1999; McIntyre and Grill, 2000; Richardson et al., 2000). The current density and the electric field around microelectrodes of various geometries have also been modeled by finite element methods. In most cases, idealized field distributions and cell shapes as well as ideal electrode properties have been assumed. McIntyre and Grill (2001) assumed a constant potential applied to the electrode metal. However, it has to be mentioned that the electrodes modeled in that study were much smaller than those used for DBS in rats. At distances as little as 50 μ m from the electrode surface, i.e. at cellular dimensions, the results were comparable to those obtained by a point source model like the one used in an earlier analysis by that group (McIntyre and Grill, 1999). Our study deals with commercially available microelectrodes of a more complex geometry, some of them previously used in DBS experiments (Windels et al., 2000, 2003; Meissner et al., 2000, 2001; Paul et al., 2000; Bruet et al., 2001; Bressand et al., 2002; Chang et al., 2003; Moser et al., 2003). Nevertheless, for larger electrodes of the same

shape the field distribution would also scale with the electrode size and, though at a larger distance, finally approach that induced by a point charge.

In our first manuscript, we focused on electrochemical electrode properties and the effects of electrode processes (Gimsa et al., 2005). The electrochemical properties are determined by electrode material, medium properties and stimulation parameters, but also (and significantly) by their geometries. Electrochemical processes caused a drift in the electrode properties within minutes and up to about 60 h, accompanied by the adsorption of organic molecules as well as metal corrosion and erosion of the plastic insulation. Generally, an electrode current causes a potential difference at both sides of the metal–medium interface, a so-called “overpotential”. Overpotentials are caused by electrochemical reactions (see Anderson and Weiland, 2002; Gimsa et al., 2005 and references cited therein). In the present study, we correlate the degradation of electrode metal and plastic insulation to numerical results on the local current density at the electrode surfaces (Figs. 7 and 8).

In animal experiments, electrodes are usually driven in a constant-current mode. This mode is intended to induce a temporal rectangular field behavior, identical to that of the applied current. The rationale is that a linear current–voltage relation of the stimulated tissue will lead to a compensation of

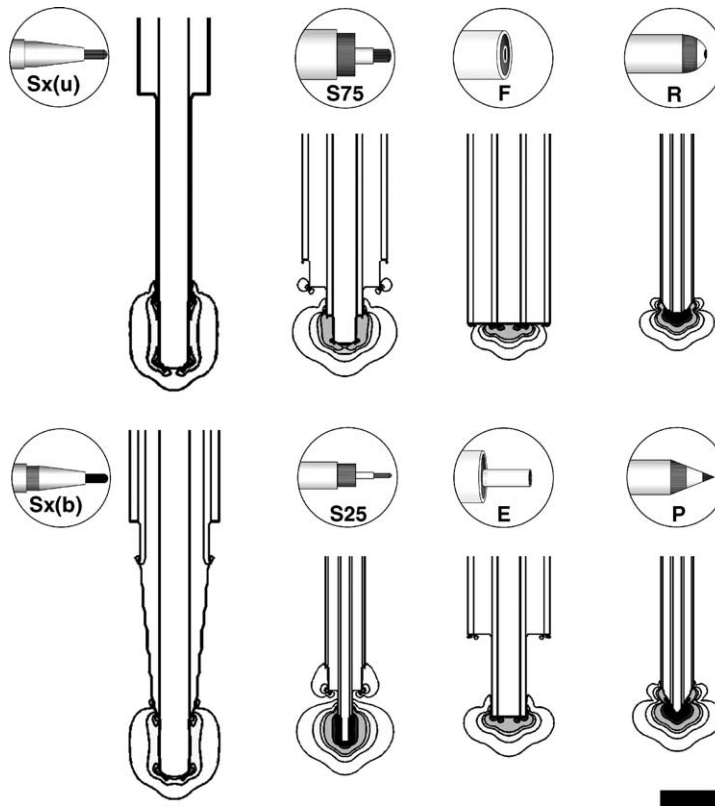


Fig. 6. Spatial distribution of the activating function, i.e. the second spatial derivative of the potential. The isolines stand for 1, 3.3, 6.7, 10, 33 and $67 \times 10^7 \text{ V/m}^2$, respectively, starting from the outermost lines. Scale bar: 200 μm .

the overpotentials by an increased electrode voltage, so allowing a constant current to flow through the tissue. Accordingly, the temporal tissue field function should be determined by the current function. Nevertheless, the local overpotentials depend on the local current densities at the different sites of the electrode surface. Consequently, the temporal field behavior in the tissue should vary with site (see below).

Overpotentials have been neglected in our numerical description of the field induced in the surrounding tissue. Under these ideal conditions, a linear current–voltage relation can be established for every electrode geometry. The proportionality factors are given by the electrode–cell constants (Eq. (1), Table 2) and the conductivities of the media. This allows for a direct calculation of the electrode voltage corresponding to a specific drive current (e.g. of the electrode voltage at a constant current of 500 μA , such as is often applied in animal models—see Section 2).

4.2. Description of the field distribution

In DBS the electrode size is roughly 10% of the brain nucleus that contains the tissue region to be stimulated. Unlike the smaller electrodes in McIntyre and Grill’s analysis (McIntyre and Grill, 1999), DBS electrodes are of a similar size or slightly larger than neurons, including their neurites. Nonetheless, the neurons in the vicinity of the electrodes experience a field distribution whose inhomogeneity plays

a role in cellular DBS effects (Kuncel and Grill, 2004). The field and current density distributions correspond for an electrically homogeneous tissue. Accordingly, field strength and current density hot spots found at electrode tips and edges are identical. The most pronounced electric cell stimulation effects as well as the highest intensities of electrochemical processes occur here. The latter processes make these sites ‘hot spots’ for the generation of toxic products and for the corrosion of electrode metal as well as the erosion of the insulation material (compare Figs. 7 and 8). One recent study has shown oxidative stress effects of iron chloride injection into

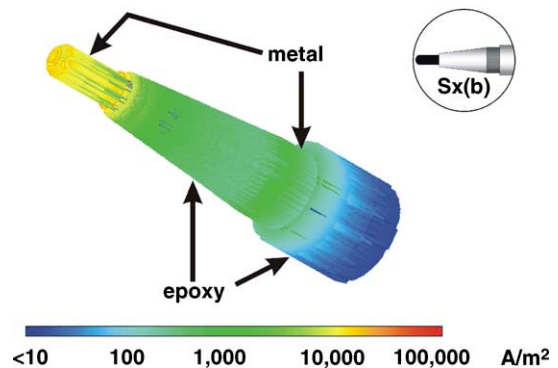


Fig. 7. Spatial distribution of the current density at the surface of a SNEX-100 (Sx(b)) electrode in aqueous solution of 1.5 S/m at 1 V.

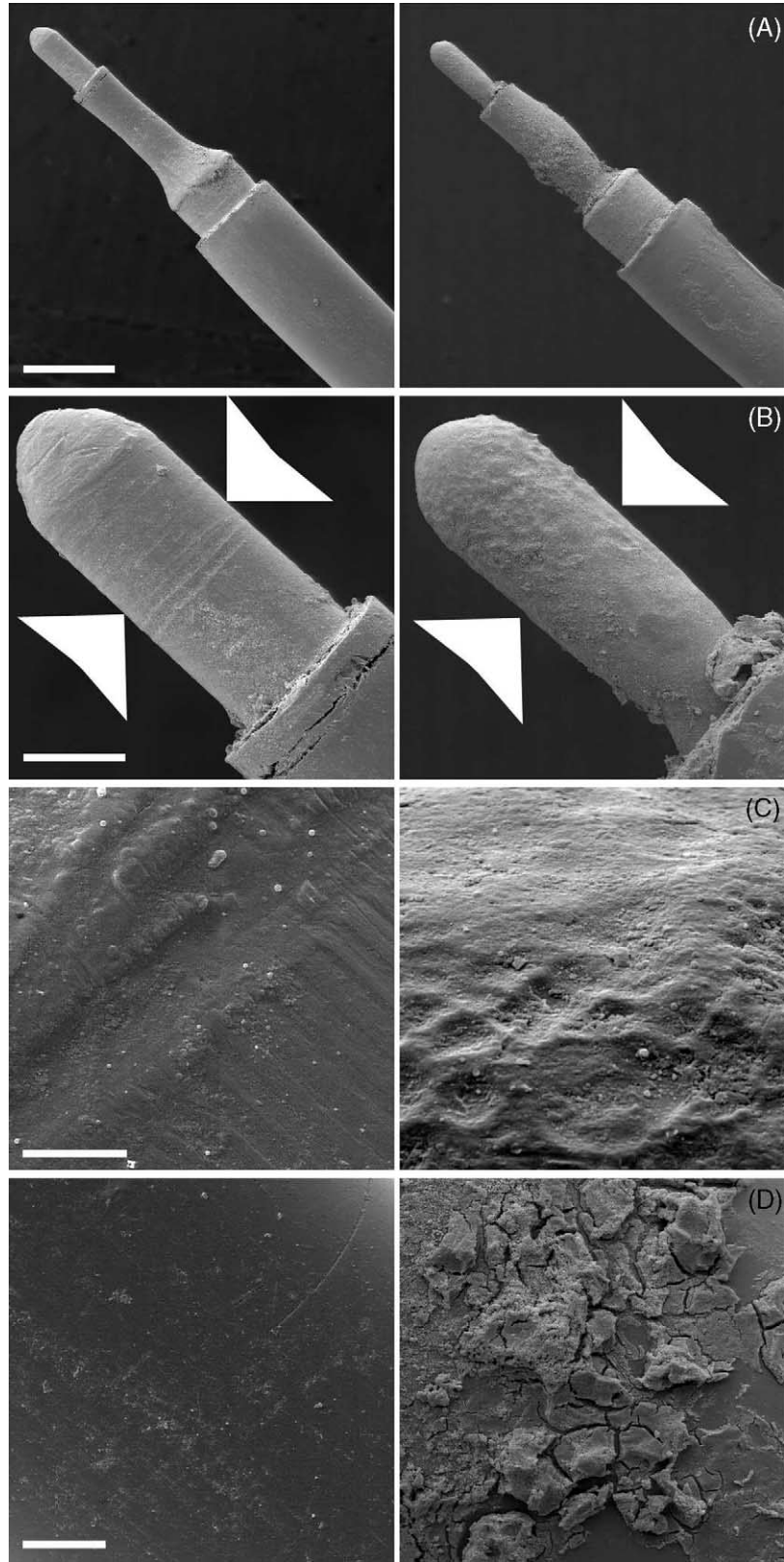


Fig. 8. Scanning electron microscopy images of a stainless steel SNEX-100 (Sx(b)) electrodes before (left panels) and after (right panels) about 8 h of stimulation in isotonic cell culture medium containing 10% fetal bovine serum. The strongest metal corrosion has been observed at the electrode tip and the interface between inner pole and insulation (compare to Fig. 7). The strongest erosion of the epoxy insulation occurred at the interface between insulation and outer pole. Images of different resolution; scale bars in A, B, C and D are 300, 70, 5 and 20 μm , respectively.

the striatum, which were neurotoxic at the site of injection. A surprising effect was the induction of immediate early gene expression in downstream nuclei of the basal ganglia network and astrogliosis (Hironishi et al., 1999). This effect might be of relevance to the gene expression analyses of DBS effects performed with stainless steel electrodes (Salin et al., 2002).

The non-uniformity of the field over the surface of the inner pole of the electrode will make positioning the electrode a delicate matter in the event of the co-localization of excitatory and inhibitory structures. Such a situation may explain why some researchers come across DBS induced inhibitory effects while others find activation of the same basal ganglia targets (Benazzouz et al., 1995; Hashimoto et al., 2003). It has been hypothesized that these opposing results are due to an inhibition of neurons, while others assume that axons (i.e. fiber paths) are activated (Vitek, 2002; McIntyre et al., 2004).

4.3. Geometry of the stimulated area

It is not yet known which neuronal elements are stimulated in DBS (McIntyre et al., 2004). As mentioned above, the induced transmembrane potential is discussed as one parameter that describes neuronal activation. It is proportional to the field strength induced in the tissue, i.e. to the current density in an assumedly homogeneous external medium. It further depends on the field frequency, cell geometry and size, as well as the electric cell and media properties (Marszalek et al., 1990; Gimsa and Wachner, 2001a). Generally, a linear relation of the induced transmembrane potential to the field strength is assumed. The maximum transmembrane potential is given by Eq. (2). Nevertheless, neuronal activity is probably influenced by the induction of comparatively low transmembrane potentials of a few mV (Warman et al., 1992). A rescaling of the transmembrane potential isolines in Figs. 4 and 5 might be necessary if a different excitation threshold is assumed (McIntyre et al., 2004). A change of the actual size of the brain tissue subject to stimulation would also occur if one considers experimental and modeling evidence for the stimulation in the cylindrical axons (Nowak and Bullier, 1998; McIntyre and Grill, 1999). Nevertheless, the transmembrane potential isolines can easily be rescaled. For objects of cylindrical shapes, the factor 1.5 in Eq. (2) must be replaced by factors of 2 and 1, respectively, when the field is oriented perpendicularly and parallel to the symmetry axis (Gimsa and Wachner, 2001b). For cells of the general ellipsoidal geometry and complex electric properties, please refer to Gimsa and Wachner (2001a).

In any case, it is important to keep the transmembrane potential below 1 V to avoid irreversible cell damage by membrane poration. In view of that, the reach of a given electrode design cannot simply be increased by increasing the electrode voltage. For electrodes P and R, the 1 V limit is already exceeded at a current of 500 μ A (Fig. 4). An additional 1 V-isopotential line (dotted) is plotted close to the surface of these electrodes. The 1 V condition (see Eq. (2)) has been used for calculating the maximum reach for all electrode

designs (Fig. 5). However, the limiting areas in the figures should be understood as qualitative estimates. Nevertheless they are useful, as the exact modeling of all tissue properties would only change the scaling, which would still allow for a semi-quantitative comparison between different electrode geometries.

Rattay et al. (2003) have derived an alternative criterion for the neuronal stimulation efficiency from phenomenological observations. These authors defined an activating function, which is the second derivative of the electric potential along a straightened axon. The first derivative of the potential along the axon describes the potential difference for a given distance along the axon, i.e. the field. A constant field, corresponding to a vanishing activating function, results in a constant current flowing in the external medium. Under these conditions, an alternating external field induces a capacitive membrane charging along the axon that will steadily follow the field alterations. At each moment the external charges along the axon will be evenly distributed. Thus the second derivative of the potential, i.e. the activating function, is non-zero at sites at which the field is not constant. Here additional charges are induced, forming sources or sinks of field. For a straightened axon these additional charges must be transported perpendicular to the axonal membrane and thus either through or towards the membrane. It can be speculated that these “additionally injected” charges are very effective in the induction of action potentials and thus for neuronal stimulation. Nevertheless, Rattay et al. (2003) derived the activating function from a resistor–capacitor ansatz that cannot directly be transformed to a three-dimensional discretized model. Since the orientation of the nerve fibers (axons) is not known, a random orientation can be assumed for simplicity. Accordingly, we calculated the second spatial derivative of the potential, i.e. the field inhomogeneity, for a homogeneous medium (Fig. 6). For this assumption, the stimulation of axons with a “correct” orientation are described according to the model of Rattay et al. (2003). Other axons are stimulated less effectively or not at all. Qualitatively, the overall picture of the activating function in the tissue will be correct (compare also to Kuncel and Grill, 2004).

Nevertheless, giving consideration only to the inhomogeneity of the external field in a homogeneous medium but not the inhomogeneities of the tissue and cell structures will probably result in an underestimation of the activating function. The reason is that the activation function may also deviate from zero in a homogeneous external field at sites of electric inhomogeneities, such as axon endings or bends. Another consideration is that a homogeneous external field will induce a transmembrane potential with opposite signs at the two sides of the cell or axon. Even though the sum is zero, an action potential can be induced because of the nonlinear membrane properties. Additionally, the two sites with a positive and negative transmembrane potential are separated by a distance that not only depends on the size but also on the orientation of the cell or axon. Whereas the two sites will be separated by the axon diameter in an axon with an orientation

of the symmetry axis perpendicular to the external field, the distance will be increased for smaller angles of orientation. For these reasons, we hypothesize that the actual distribution of the neuronal stimulation efficiency in the tissue is a complex blend of various parameters with contributions of the field strength and activating function distributions.

4.4. Stimulation parameters and cell stimulation

The complex relations at the electrodes and in the surrounding tissue call for measurable parameters for standardizing the DBS procedure when transferred from humans to animals or between electrode geometries. Even though the stimulation effect is only related to the induced tissue field or current, i.e. charges that are actually transferred into the tissue, frequently charge densities and charge per phase are used to derive limiting stimulation values (Harnack et al., 2004). However, these parameters, for instance the recommended Medtronic® average charge density limit of $30 \mu\text{C}/\text{cm}^2$, refer to the well-defined electrodes used in human therapy. Nevertheless, even for these large, smoothly shaped electrodes, the charge density distribution at the electrode surface is inhomogeneous (Kuncel and Grill, 2004). Accordingly, the average charge density is not an appropriate parameter for describing the field induced in the tissue, and it has a limited potential for transferring stimulation parameters to electrodes of other geometries. By contrast, numerically calculated current densities take into account geometric aspects of charge distribution along the surface and reveal critical features related to size and curvature of electrodes.

However, both the assumption of charge densities and our present calculations neglect two current contributions. First, the electrode capacity will be charged. This capacity cannot simply be derived from the geometry and the permittivity of the surrounding medium but will be dominated by reversible electrochemical processes similar to those in an electrolytic capacitor. Second, and even more important for a correct description are overpotentials. These are generated by irreversible electrochemical reactions like redox processes related to the transition of electronic to ionic conductance for a current passing from metal to electrolyte medium, i.e. tissue. An overpotential is then defined as the potential difference between the electrode and the surrounding medium. However, the related processes are very complicated (see Gimsa et al., 2005 and references cited therein).

For a dc or low frequency signal, the local overpotential along the electrode surface will depend on the local current density since it is based on the intensity of the local electrochemical reactions. On the other hand, ongoing electrochemical reactions will reduce the effective impedance for the local electrode current. Therefore, at sites of high current densities, such as electrode tips and edges, the specific potential drop will be lowered according to Ohm's law, probably smoothening the potential and field distributions in the tissue with respect to the numerical results. It was not possible to take these processes into account when calculating the cell

constants (Table 2). Therefore, the obtained constants will only be correct for frequencies at which electrode processes are capacitively bridged. In practice, the overpotentials will alter the current–voltage relation and require corrections for the constants that will depend on amplitude and frequency content of the stimulation pulse. It should be mentioned that extrapolation of the experimental impedance semi-circle to dc yields a resistance corresponding to that given in Table 2 for the S75 electrode. For details, see Gimsa et al. (2005).

4.5. Frequency dependence of the field strength distribution

The current or voltage pulses used in DBS contain an infinite number of harmonic frequencies. Therefore, we propose describing the DBS pulses by Fourier series (Gimsa et al., 2005). All the same, a separate consideration of continuous sinusoidal currents or voltages applied to the electrode will only be correct if the strong nonlinearities of the overpotentials are neglected. Such a simplified approach will permit a description of field propagation in the tissue based on the frequency-dependent tissue impedance. For every site in the tissue, the field amplitude and time dependence can be reconstructed from the sum of the amplitudes of each Fourier component. Nevertheless, a correct description of the potential drop over the interfacial impedance for each frequency component is difficult for three reasons.

First, the overpotentials of each frequency component exhibit a nonlinear current–voltage relation, resulting in the generation of nonlinear distortions—especially for the low frequency components.

Secondly, the overpotential for each frequency component depends on the actual overall current through the electrode surface; and thirdly, the electrode properties depend on the history of the electrodes (Gimsa et al., 2005).

Furthermore, a rectangular constant current pulse through the electrode may induce field pulses of different shapes at different electrode sites. The reason is the impedance distribution along the electrode surface, i.e. different overpotentials and different degrees of capacitive bridging of the overpotentials for the frequency components of the signal. Accordingly, the tissue near the electrode will experience different current wave forms, i.e. different time functions of the tissue field, even though the different local surface current contributions must add up to the (rectangular) constant current input pulse.

The importance of the two effects, i.e. the site-dependent current density and, even more complicated, the current density-dependent frequency dependence of the overpotentials for DBS is not (yet) clear. An analytical description might require an iterative approach. For this, the calculation of the current density distribution at the electrode surface will be the first iterative step. In a second step, based on the current density distribution, an overpotential distribution could be calculated which could then serve to correct the current density distribution, and so on. However, the result of this

approach cannot describe the time or frequency-dependent properties of the overpotentials or the influence of molecular adsorption, gas bubble formation, metal corrosion, etc. on the electrode properties. Moreover, also the electric brain tissue properties are anisotropic and inhomogeneous (Grill, 1999). Another unsolved problem is the frequency dependence of the spreading of the stimulation signal in the brain tissue. Cell membranes, cytoplasmic structures and interstitial media form frequency filters changing the frequency spectrum in the stimulated tissue in dependence on the electrode distance. To solve all these problems is far beyond the scope of this manuscript and would require new experimental approaches and complex programming.

4.6. Relevance to human electrodes

A study on the field around medical DBS electrodes has recently been published (Kuncel and Grill, 2004). Even though the design and materials as well as the stimulation protocols of the medical electrodes differ from those used in animal experiments, the principles presented in our studies are also practical for describing the field distribution, for deriving cell constants and assessing electrode designs. Although corrosion has not been observed with medical electrodes, electrochemical processes are unavoidable and need consideration. A respective study is currently underway.

5. Conclusions

Modeling DBS effects in their full complexity is far beyond the scope of this manuscript and requires a synthesis of the insights of this and our previous study (Gimsa et al., 2005) with neuronal DBS models drawn up by others (Grill, 1999; Horch and Dhillon, 2002 and contributions therein; McIntyre et al., 2004; Grill et al., 2004). Nevertheless, electrode geometry is the primary variable when targeting brain areas of different sizes in humans and animals. Our analysis has shown that next to electrode materials, their geometries are most important in determining stimulation parameters that are safe for the tissue. Simple down-sizing of the human electrodes while maintaining stimulation protocols is not an option. The basis for comparing different geometries must be electrode impedances, i.e. current–voltage relations. These relations are reflected in the cell constants. They increase or decrease with a characteristic dimension for electrodes of the same shape.

At the electrode surface, the field is correlated to the current density corresponding to the intensity of electrochemical processes. These processes may cause metal corrosion and plastics erosion leading to the deposition of putative neurotoxic compounds in the brain tissue, as shown here with a stainless steel electrode. However, even when noble metals and inert insulation materials are used, electrochemical processes can occur which may result in gas production, for example. Therefore, avoid tips and edges; i.e. high curvatures:

the highest current densities and field strengths are located here, which also limit the maximum current or voltage applicable without electrical tissue damage. In turn, the maximum size of the tissue stimulated is limited for a given electrode geometry. The shape of the stimulated tissue strongly depends on the geometry of the poles of the electrode, i.e. their size and position relative to each other.

Even though the inclusion of nonlinear electrode behavior in the calculations imposes a serious problem, the analysis of the local current density distribution at the electrode surface and in the surrounding tissue will help in deciding whether the electrochemical load at the electrodes is uniform and whether the tissue is uniformly stimulated.

In order to describe the stimulation effect correctly, not just the frequency dependence of the electrode processes but also the complex electric properties of the brain tissue, its inhomogeneity, and anisotropy, as well as the frequency dependence of the spread of the stimulation signal have to be taken into account. Using the tools described here, the optimal electrode can be found amongst those available on the market, in order to aim at different-sized brain targets.

Acknowledgements

This study has been supported by grants 01 ZZ 0108 from the Bundesministerium für Bildung und Forschung (Federal Ministry for Education and Research) to U.G. and StSch 2002 0418A from the Bundesamt für Strahlenschutz (Federal Office for Radiation Protection) to J.G. The authors would like to thank Prof. Dr. Frank Rattay, Vienna University of Technology, and Dr. Ulf Strauss, University of Rostock, for their helpful discussions. The cooperation of the “electron microscopy” core facility at the University of Rostock’s Medical Faculty is also acknowledged. The authors would also like to thank Robert Sleight for his help with the manuscript.

Appendix A. Numerical solution of Maxwell’s equations by FIT under the EQS approximation

The complete basis of macroscopic electromagnetic theory is formed by three material laws and the four Maxwell equations (Maxwell, 1873). With FIT (Weiland, 1977; Schuhmann et al., 1996), the continuous quantities arising in Maxwell’s equations, i.e. electric and magnetic voltages and fluxes, are computed on a finite number of grid cells: the voltages are computed along the edges and the fluxes across facets of the grid cells. While employing the material relations on the grid does require approximations, the discretization of voltages and fluxes is exact. FIT ensures that the interdependent physical relations between electric and magnetic field quantities are transferred to the grid in a very natural way. This results in a consistent model with the basic physical properties still holding on the discrete grid like energy conservation, source-free magnetic fields, etc.

Furthermore, the topologically regular grids of FIT allow for a reliable automatic mesh generation, while 3D mesh generation often fails in FEM for large problems. At the same time, the regularity of the grid allows for economical memory requirements. The geometric error is minimized even in rather coarse Cartesian grids by using diagonal fillings of grid cells when setting up the grid operators.

Eventually, a system of linear equations, the so-called Maxwell's Grid Equations, are obtained (see below).

For slowly varying time harmonic electromagnetic fields, the complexity of the problem can be reduced applying the EQS approximation. An electromagnetic field can be considered as slowly varying if the wavelength is large compared to the characteristic dimension R of the problem region. The criterion is $|kR| \ll 1$, with k standing for the complex wave number. In a lossy dielectric medium the complex wave number is $k = \omega \sqrt{\mu(\varepsilon - i(\sigma/\omega))}$ with ω , μ , ε and σ standing for the circular frequency, the magnetic permeability, the electric permittivity, and the specific conductivity, respectively. The permittivity ($\varepsilon = \varepsilon_r \varepsilon_0$) and permeability ($\mu = \mu_r \mu_0$) are defined by their vacuum (index 0) and their relative material (index r) parameters. For the electrode problem R can be assumed to be about 1 mm with a specific conductivity σ of 1.5 S/m and relative permittivity and permeability ε_r and μ_r of 80 and 1, respectively. For a frequency of 130 Hz, these parameters result in $|kR| \approx 3.9 \times 10^{-5}$, rendering the EQS problem formulation legitimate.

Nevertheless, the Fourier series of the rectangular DBS pulse contains harmonic frequencies of up to 1 MHz, though with decreasing amplitudes (see Gimsa et al., 2005). Furthermore, the material parameters are not constant in the frequency range from 100 Hz to 1 MHz. Whereas the relative permittivity and conductivity of gray matter change from 3.9×10^6 to 860 and 0.09 S/m to 0.16 S/m, these parameters change from 1.66×10^6 to 480 and 0.058 S/m to 0.102 S/m for white matter (<http://niremf.ifac.cnr.it/tissprop/htmlclie/htmlclie.htm#atsftag>). These changes result in complex wave numbers k ranging from 0.0085 to 1.1 m^{-1} for gray matter and from 0.0068 to 0.9 m^{-1} for white matter. In any case, $|kR| \ll 1$.

Also the other parameters may be found in the literature. For calculation purposes, we used the above parameters for an aqueous electrolyte such as used in cell culturing. Parameter changes would only slightly influence the resulting distributions, predominantly in the vicinity of interfaces of aqueous solution and insulation material, i.e. at the so-called triple-points.

When reducing the model to the EQS problem the time-derivative of the magnetic flux is assumed to be negligible ($\partial \mathbf{B} / \partial t \approx 0$, please note the underscore denoting complex quantities). Thus, whereas the magnetic flux variation is neglected, displacement currents are taken into account ($\partial \mathbf{D} / \partial t \neq 0$) (Haus and Melcher, 1989; Dirks, 1996). Time-harmonic EQS modelling reduces the problem size to one third as only potentials (but not vector fields) need to be computed.

For time harmonic fields the EQS approximation yields the following set of simplified Maxwell's equations:

$$\text{curl } \underline{\mathbf{E}} = 0 \quad (\text{A.1})$$

$$\text{curl } \underline{\mathbf{H}} = i\omega \underline{\mathbf{D}} + \sigma \underline{\mathbf{E}} + \underline{\mathbf{J}}_I \quad (\text{A.2})$$

$$\text{div } \underline{\mathbf{D}} = \rho \quad (\text{A.3})$$

$$\text{div } \underline{\mathbf{B}} = 0, \quad (\text{A.4})$$

with $\underline{\mathbf{H}}$, $\underline{\mathbf{E}}$, $\underline{\mathbf{B}} = \mu \underline{\mathbf{H}}$, $\underline{\mathbf{D}} = \varepsilon \underline{\mathbf{E}}$, ρ denoting the magnetic field strength, the electric field strength, the magnetic induction, the dielectric displacement and the charge density, respectively. The overall current density $\underline{\mathbf{J}} = \underline{\mathbf{J}}_I + \sigma \underline{\mathbf{E}}$ comprises the impressed current density, $\underline{\mathbf{J}}_I$, and the conduction current density, $\sigma \underline{\mathbf{E}}$. According to Eq. (A.1) the electric phasor $\underline{\mathbf{E}}$ is curl-free and may thus be described as the gradient of a scalar potential: $\underline{\mathbf{E}} = -\text{grad } \underline{\phi}$. Please note that the potential $\underline{\phi}$ is a complex quantity. It can be obtained from the complex divergence equation summarizing Eqs. (A.1)–(A.4) for the above conditions:

$$\text{div}((i\omega\varepsilon + \sigma) \text{grad } \underline{\phi}) = \text{div}(\underline{\mathbf{J}}_I). \quad (\text{A.5})$$

Eq. (A.5) is the continuity equation that is transformed into its discrete form in FIT (Weiland, 1977; van Rienen et al., 2003):

$$\tilde{\mathbf{S}}(i\omega \mathbf{M}_\varepsilon + \mathbf{M}_\sigma) \tilde{\mathbf{S}}^T \underline{\phi}_E = \tilde{\mathbf{S}} \mathbf{i}, \quad (\text{A.6})$$

with the material matrices \mathbf{M}_ε and \mathbf{M}_σ holding the permittivities and electric conductivities (van Rienen et al., 2003). $\tilde{\mathbf{S}}$ and $\tilde{\mathbf{S}}^T$ are the divergence-operator and the gradient operator, respectively, with the latter being the transposed matrix of $\tilde{\mathbf{S}}$. For isotropic media, \mathbf{M}_ε and \mathbf{M}_σ are diagonal matrices. The notations $\mathbf{A}_\varepsilon := \tilde{\mathbf{S}} \mathbf{M}_\varepsilon \tilde{\mathbf{S}}^T$ and $\mathbf{A}_\sigma := \tilde{\mathbf{S}} \mathbf{M}_\sigma \tilde{\mathbf{S}}^T$ lead to the linear system of complex equations used in the computation:

$$\mathbf{A} \underline{\phi}_E = \tilde{\mathbf{S}} \mathbf{i}. \quad (\text{A.7})$$

The matrix $\mathbf{A} := (\mathbf{A}_\sigma + i\omega \mathbf{A}_\varepsilon)$ is a large sparse symmetric matrix with seven bands. To solve Eq. (A.7) we applied state-of-the-art Krylov subspace methods (van Rienen, 2001). Finally, all physical quantities such as the electric field strengths or the current densities can be computed from the discrete FIT operators in the post-processing.

References

- Agnew WF, McCreery DB. Neural Prostheses: Fundamental Studies. Englewood Cliffs, NJ: Prentice Hall Inc; 1990.
- Anderson DJ, Weiland J. Neural stimulation electrodes: geometric factors. In: Horch KW, Dhillon GS, editors. Neuroprosthetics: theory and practice. World Scientific Publishing; 2002.
- Benabid AL, Pollak P, Louveau A, Henry S, de Rougemont J. Combined (thalamotomy and stimulation) stereotactic surgery of the VIM thalamic nucleus for bilateral Parkinson disease. Appl Neurophysiol 1987;50:344–6.

- Benazzouz A, Piallat B, Pollak P, Benabid AL. Responses of substantia nigra pars reticulata and globus pallidus complex to high frequency stimulation of the subthalamic nucleus in rats: electrophysiological data. *Neurosci Lett* 1995;189:77–80.
- Bressand K, Dematteis M, Ming GD, Vercueil L, Louis BA, Benazzouz A. Superior colliculus firing changes after lesion or electrical stimulation of the subthalamic nucleus in the rat. *Brain Res* 2002;943:93–100.
- Bruet N, Windels F, Bertrand A, Feuerstein C, Poupard A, Savasta M. High frequency stimulation of the subthalamic nucleus increases the extracellular contents of striatal dopamine in normal and partially dopaminergic denervated rats. *J Neuropathol Exp Neurol* 2001;60:15–24.
- Chang JY, Shi LH, Luo F, Woodward DJ. High frequency stimulation of the subthalamic nucleus improves treadmill locomotion in unilateral 6-hydroxydopamine lesioned rats. *Brain Res* 2003;983:174–84.
- Darbaky Y, Forni C, Amalric M, Baunez C. High frequency stimulation of the subthalamic nucleus has beneficial antiparkinsonian effects on motor functions in rats, but less efficiency in a choice reaction time task. *Eur J Neurosci* 2003;18:951–6.
- Dirks HK. Quasi-stationary fields for microelectronic applications. *Electr Eng* 1996;79:145–55.
- Gimsa J, Glaser R, Fuhr G. Remarks on the field distribution in four electrode chambers for electrorotational measurements. *Studia Biophys* 1988;125:71–6.
- Gimsa J, Habel B, Schreiber U, van Rienen U, Strauss U, Gimsa U. Choosing electrodes for deep brain stimulation experiments—electrochemical considerations. *J Neurosci Methods* 2005;142:251–65.
- Gimsa J, Wachner D. Analytical description of the transmembrane voltage induced on arbitrarily oriented ellipsoidal and cylindrical cells. *Biophys J* 2001a;81:1888–96.
- Gimsa J, Wachner D. On the analytical description of transmembrane voltage induced on spheroidal cells with zero membrane conductance. *Eur Biophys J* 2001b;30:463–6.
- Grill WM. Modeling the effects of electric fields on nerve fibers: influence of tissue electrical properties. *IEEE Trans Biomed Eng* 1999;46:918–28.
- Grill WM, Mortimer JT. The effect of stimulus pulse duration on selectivity of neural stimulation. *IEEE Trans Biomed Eng* 1996;43:161–6.
- Grill WM, Snyder AN, Miocinovic S. Deep brain stimulation creates an informational lesion of the stimulated nucleus. *Neuroreport* 2004;15:1137–40.
- Haberler C, Alesch F, Mazal PR, Pilz P, Jellinger K, Pinter MM, et al. No tissue damage by chronic deep brain stimulation in Parkinson's disease. *Ann Neurol* 2000;48:372–6.
- Harnack D, Winter C, Meissner W, Reum T, Kupsch A, Morgenstern R. The effects of electrode material, charge density and stimulation duration on the safety of high-frequency stimulation of the subthalamic nucleus in rats. *J Neurosci Methods* 2004;138:207–16.
- Hashimoto T, Elder CM, Okun MS, Patrick SK, Vitek JL. Stimulation of the subthalamic nucleus changes the firing pattern of pallidal neurons. *J Neurosci* 2003;23:1916–23.
- Haus HA, Melcher JR. *Electromagnetic fields and energy*. Prentice Hall Inc; 1989.
- Henderson JM, Pell M, O'Sullivan DJ, McCusker EA, Fung VS, Hedges P, et al. Postmortem analysis of bilateral subthalamic electrode implants in Parkinson's disease. *Mov Disord* 2002;17:133–7.
- Hironishi M, Ueyama E, Senba E. Systematic expression of immediate early genes and intensive astrocyte activation induced by intrastriatal ferrous iron injection. *Brain Res* 1999;828:145–53.
- Horch KW, Dhillon GS. *Neuroprosthetics: theory and practice*. World Scientific Publishing; 2002.
- Kuncel AM, Grill WM. Selection of stimulus parameters for deep brain stimulation. *Clin Neurophysiol* 2004;115:2431–41.
- Marszalek P, Liu DS, Tsong TY. Schwan equation and transmembrane potential induced by alternating electric field. *Biophys J* 1990;58:1053–8.
- Maxwell JC. *Treatise on electricity and magnetism*. London: Oxford University Press; 1873.
- McIntyre CC, Grill WM. Excitation of central nervous system neurons by nonuniform electric fields. *Biophys J* 1999;76:878–88.
- McIntyre CC, Grill WM. Selective microstimulation of central nervous system neurons. *Ann Biomed Eng* 2000;28:219–33.
- McIntyre CC, Grill WM. Finite element analysis of the current-density and electric field generated by metal microelectrodes. *Ann Biomed Eng* 2001;29:227–35.
- McIntyre CC, Grill WM, Sherman DL, Thakor NV. Cellular effects of deep brain stimulation: model-based analysis of activation and inhibition. *J Neurophysiol* 2004;91:1457–69.
- Meissner W, Paul G, Reum T, Reese R, Sohr R, Morgenstern R, et al. The influence of pallidal deep brain stimulation on striatal dopaminergic metabolism in the rat. *Neurosci Lett* 2000;296:149–52.
- Meissner W, Reum T, Paul G, Harnack D, Sohr R, Morgenstern R, et al. Striatal dopaminergic metabolism is increased by deep brain stimulation of the subthalamic nucleus in 6-hydroxydopamine lesioned rats. *Neurosci Lett* 2001;303:165–8.
- Moser A, Gieselberg A, Ro B, Keller C, Qadri F. Deep brain stimulation: response to neuronal high frequency stimulation is mediated through GABA(A) receptor activation in rats. *Neurosci Lett* 2003;341:57–60.
- Moss J, Ryder T, Aziz TZ, Graeber MB, Bain PG. Electron microscopy of tissue adherent to explanted electrodes in dystonia and Parkinson's disease. *Brain* 2004;127:2755–63.
- Nowak LG, Bullier J. Axons, but not cell bodies, are activated by electrical stimulation in cortical gray matter. II. Evidence from selective inactivation of cell bodies and axon initial segments. *Exp Brain Res* 1998;118:489–500.
- Paul G, Reum T, Meissner W, Marburger A, Sohr R, Morgenstern R, et al. High frequency stimulation of the subthalamic nucleus influences striatal dopaminergic metabolism in the naive rat. *Neuroreport* 2000;11:441–4.
- Rattay F, Resatz S, Lutter P, Minassian K, Jilge B, Dimitrijevic MR. Mechanisms of electric stimulation with neural prostheses. *Neuro-modulation* 2003;6:42–56.
- Richardson AG, McIntyre CC, Grill WM. Modelling the effects of electric fields on nerve fibres: influence of the myelin sheath. *Med Biol Eng Comput* 2000;38:438–46.
- Salin P, Manrique C, Forni C, Kerkerian-Le Goff L. High-frequency stimulation of the subthalamic nucleus selectively reverses dopamine denervation-induced cellular defects in the output structures of the basal ganglia in the rat. *J Neurosci* 2002;22:5137–48.
- Schuhmann R, Clemens M, Thoma P, Weiland T. Frequency and time domain computations of S-parameters using the finite integration technique. In: *Proceedings of the 12th Annual Review of Progress in Applied Computational Electromagnetics (ACES Conference)*; 1996. p. 1295–302.
- Suzuki T, Shin BC, Fujikura K, Matsuzaki T, Takata K. Direct gene transfer into rat liver cells by in vivo electroporation. *FEBS Lett* 1998;425:436–40.
- van Rienen U. Numerical methods in computational electrodynamics—linear systems in practical applications. In *Lecture Notes in Computational Science and Engineering*. Springer; 2001.
- van Rienen U, Flehr J, Schreiber U, Motrescu V. Modeling and simulation of electro-quasistatic fields. *Int Series Numer Math* 2003;146:17–31.
- Vitek JL. Mechanisms of deep brain stimulation: excitation or inhibition. *Mov Disord* 2002;17(Suppl. 3):S69–72.
- Warman EN, Grill WM, Durand D. Modeling the effects of electric fields on nerve fibers: determination of excitation thresholds. *IEEE Trans Biomed Eng* 1992;39:1244–54.
- Weiland T. A discretization method for the solution of Maxwell's equation for six-component fields. *Electron Commun AEU* 1977;31:116–20.

Windels F, Bruet N, Poupard A, Feuerstein C, Bertrand A, Savasta M. Influence of the frequency parameter on extracellular glutamate and gamma-aminobutyric acid in substantia nigra and globus pallidus during electrical stimulation of subthalamic nucleus in rats. *J Neurosci Res* 2003;72:259–67.

Windels F, Bruet N, Poupard A, Urbain N, Chouvet G, Feuerstein C, et al. Effects of high frequency stimulation of subthalamic nucleus on extracellular glutamate and GABA in substantia nigra and globus pallidus in the normal rat. *Eur J Neurosci* 2000;12:4141–6.